Radiocarbon, Vol 62, Nr 3, 2020, p 713–724 DOI:10.1017/RDC.2020.48
Selected Papers from the Mortar Dating International Meeting, Pessac, France, 25–27 Oct. 2018

RADIATION DEFECTS IN LIME MORTARS AND PLASTERS STUDIED BY EPR SPECTROSCOPY

Zuzanna Kabacińska[1]* • Danuta Michalska[2] • Bernadeta Dobosz[3]

[1]Institute of Chemistry and Technical Electrochemistry, Poznań University of Technology, Berdychowo 4, 60-965 Poznań, Poland
[2]Institute of Geology, Faculty of Geographical and Geological Sciences, Adam Mickiewicz University, Krygowskiego 12, 61-680 Poznań, Poland
[3]Medical Physics and Radiospectroscopy Division, Faculty of Physics, Adam Mickiewicz University, Uniwersytetu Poznańskiego 2, 61-614 Poznań, Poland

ABSTRACT. Electron paramagnetic resonance (EPR) spectroscopy is a well-established method of dating based on trapped charges, applied to various crystalline materials, including carbonates, bones, and teeth. It provides a detailed insight into the structure of radiation defects—paramagnetic centers generated by irradiation, without the need of a painstaking sample preparation, often challenging in other methods. Using EPR we studied the effect of γ radiation on lime mortars and plasters from ancient settlement Hippos in Israel, in order to analyze the process of defect generation. Analysis of the complex spectra revealed the presence of radiation-induced species, including CO_2^-, NO_3^{2-} and organic radical. Using an artificial UV source, we generated relatively strong signals of paramagnetic centers, analogous to those created by γ irradiation, reaching their maximum intensity after 5–6 hr of UV exposure. Our results confirm the previous reports that radiation defects can also be generated, instead of bleached, in calcite by UV radiation, which is crucial for identifying the issues related to light exposition, affecting the accuracy of age determinations in trapped-charge dating methods.

KEYWORDS: calcite, EPR, mortar, radiation defects, UV light.

INTRODUCTION

Fast development in radiocarbon (^{14}C) and optically stimulated luminescence (OSL) mortar dating naturally widens the scope of performed analysis (Panzeri 2013; Ringbom et al. 2014; Hajdas et al. 2017; Michalska et al. 2017; Urbanová and Guibert 2017), and promotes the search for different methods, which may shed some light on the previously unconsidered aspects of mortar dating. In order to meet the growing need of understanding the complexity of composition and gradual structural changes in this material, the insight in its physics and chemistry is necessary. Electron paramagnetic resonance (EPR, also called electron spin resonance—ESR) spectroscopy, with its high sensitivity and tremendous potential for providing detailed structural information seems to be an ideal candidate for a new addition to mortar analyses.

EPR is a well-established method of dating, applied to various crystalline materials, such as calcium carbonate. It provides a detailed insight into the structure of radiation defects—paramagnetic centers generated by irradiation, without the need of a painstaking sample preparation, often challenging in other methods. EPR dating is built on the same principle as the luminescence techniques—trapping of charges (electrons and holes). When high-energy radiation (e.g. γ, X-ray) irradiates a crystal, it excites an electron from the valence band to the conduction band. The electron and hole then diffuse and become trapped in additional energy levels in the forbidden band, typically caused by imperfections of the crystal lattice, thus creating a paramagnetic center. These centers are detected in an EPR experiment, when the sample is placed in a homogeneous magnetic field and irradiated by a continuous flow of microwaves, which, when resonance condition is fulfilled, entails a transition between two spin states. (Grün 1991; Ikeya 1993, 2004)

*Corresponding author. Email: zuziakab@amu.edu.pl.

Although the effects of γ radiation on calcium carbonate, especially in the form of calcite, has been investigated very thoroughly (Ikeya 1993, 2004; Bahain et al. 1994; Callens 1997; Callens et al. 1998; Baïetto et al. 1999; Polikreti et al. 2004; Wencka et al. 2005; Kabacińska et al. 2017, 2019), to our knowledge only our group has analyzed it in lime mortars, first on samples from Sveta Petka church in Budinjak, Croatia (Kabacińska et al. 2012), and later from ancient settlement Hippos, Israel (Kabacińska et al. 2014b). In these studies, we found several signals generated in lime mortars by γ radiation and examined the dose response curves. Since those samples were not suitable for EPR dating, because of their relatively young (for this technique) age, and the collection method (suitable for ^{14}C, but not for trapped-change dating), we focused only on their physicochemical properties, and not age determination (^{14}C dates can be found in Michalska 2019 and Michalska and Pawlyta 2019). Research conducted during the last few years by the main author and coworkers (Kabacińska et al. 2014a, 2017, 2019) as well as a few different groups (Bartoll et al. 2000; Sato et al. 2004; Kundu et al. 2005) clearly show that radiation defects can also be generated in calcite, instead of bleached, by UV radiation. Recently (Kabacińska et al. 2017, 2019), we proposed a mechanism of UV-induced generation of radiation defects in calcite, based on trapping the "secondary electrons"—electrons freed from non-carbonate traps by the incident UV radiation. These studies were conducted on high-purity calcite samples, which provoked the need to investigate this phenomenon for carbonate materials containing more impurities, occurring in archaeological and geological contexts. We have chosen the samples of mortars and plasters from Hippos because their response to γ irradiation has been previously studied and therefore they provide a good basis for comparison. In this work we analyze the effect of UV exposure on these materials by comparing the UV- and γ-generated centers and provide the additional interpretation of the signals reported in our previous work on Hippos samples. Our results can lead to a deeper understanding of generation and bleaching mechanisms of paramagnetic species, which is crucial for identifying the issues, especially related to light exposition, affecting the accuracy and precision of mortar dating.

EXPERIMENTAL

Sample Collection

Our studies were conducted on lime mortars and plasters from the ancient settlement of Hippos in Israel. Hippos (Sussita) was situated on the east shore of the Sea of Galilee. It was founded in the 3rd century BC and functioned until 749 AD when it was destroyed by an earthquake.

Samples Hip 8 and Hip10 are pure lime plasters form the central apse (west wall) and the southern aisle (by the balustrade, northern face) of the North-West church (NWC), respectively. ^{14}C dating of the sample Hip 10 gave the age 1245 ± 35 BP (AMS, Poz-7417) and 1310 ± 45 BP (GPC, Gd-12823) (Michalska Nawrocka et al. 2007), consistent with the archeological estimations. Hip 61 it is a carbonate mortar with a carbonaceous-basaltic aggregate, taken from the northern wall of the facade of the pastophorium, NWC. Few samples (bulk material, grain fraction, suspension) of this mortar were ^{14}C dated using different pretreatment methods, giving the results: 1080 ± 100 (Gd-18388), 1490 ± 30 (Poz-16078) (Michalska Nawrocka et al. 2007; Michalska 2019), 7140 ± 90 (Gd-12824) (Michalska 2019; Michalska and Pawlyta 2019), 1795 ± 30 (Poz-97829), and 1470 ± 30 BP (Poz-97862) (Michalska 2019).

Detailed information about the site, the precise location of sample collection points and the applied ^{14}C dating preparation technique can be found in Nawrocka et al. (2005, 2009);

https://doi.org/10.1017/RDC.2020.48 Published online by Cambridge University Press

Michalska Nawrocka et al. (2007); Kabacińska et al. (2014b); Michalska (2019); Michalska and Pawlyta (2019).

Sample Preparation and Irradiation

Samples for EPR measurements were gently crushed and fragments of aggregate bigger than 2 mm were removed under a stereomicroscope. Sample 61H is a sieved fraction 63–80 μm of original sample Hip61, while samples Hip8 and Hip10 were not sieved.

UV irradiation was performed under air conditions using medium pressure Hg lamp EMITA VP – 60 (Farmed, Łodź, Poland) working at 180 W, used without a filter, and lasted from 30 min to 7.5 hr, divided in 4 series with a 1–10-week gap between them. The spectral output of the lamp was in the 238–577 nm range, with main wavelengths 313 nm and 366 nm (spectrum shown in Kabacińska et al. 2019; see Supplementary Information). During UV exposure, the samples were placed under the maximum irradiation point, 10.5 cm from the source, and flattened to form a thin layer (~0.5 mm in thickness) covering the irradiated area. The temperature under the lamp at the sample position did not exceed 65ºC during irradiation. All three samples were γ-irradiated using ^{60}Co source with doses of 1, 10, 20, 50, 80, and 100 kGy at the Institute of Applied Radiation Chemistry, Technical University of Łódź, and sample 61H additionally with doses of 50, 100, 300, 500, 800, 2210, and 3000 Gy, at the Institute of Molecular Physics, Polish Academy of Sciences in Poznań (see Kabacińska et al. 2014b).

Characterization Techniques

The macroscopic fragments of samples as well as thin sections were examined with stereomicroscope and polarizing light microscope Olympus AX 70-Prons. XRD analyses were conducted on Thermo Electron ARL X'tra diffractometer, using Cu Kα radiation at scanning speed 2Theta = 1.2°/min. Different mineralogical phases were identified using Win XRD software.

EPR measurements were performed at room temperature with an X-band Bruker spectrometer (EMX type), working at 9 GHz, with ER 4102ST standard rectangular cavity (model TE_{102}). Standard parameters for measurements in 15 mT scan range were: 10^5 receiver gain, 7.950 mW microwave power, 0.05 mT modulation amplitude, 81.920 ms conversion time and time constant, 100.00 kHz modulation frequency. The magnetic field was measured with a gaussmeter and the frequency with a frequency counter (with accuracy ± 0.001 G and ± 0.001 GHz respectively). The *g*-factor was calculated from these values and verified by measuring DPPH and weak pitch standard samples. The uncertainty of *g*-factor was estimated as ± 0.0003. Each sample weighted 100.0 ± 0.5 mg. UV-irradiated samples were put in an EPR tube and measured within 5 min from the end of exposure (with an exception of the first measurement of each series, which did not involve an UV irradiation). The WINEPR SimFonia 1.25 software (Bruker Analytische Messtechnik GmbH) with powder model was used for the simulation of the EPR signals.

RESULTS AND DISCUSSION

Sample Characterization

All presented mortar samples had carbonaceous binders. Microscopic analysis of as-collected samples Hip 8 and Hip10 showed they are almost devoid of any aggregate, with only small fragments of not totally burnt raw material and empty spaces left after straw present

https://doi.org/10.1017/RDC.2020.48 Published online by Cambridge University Press

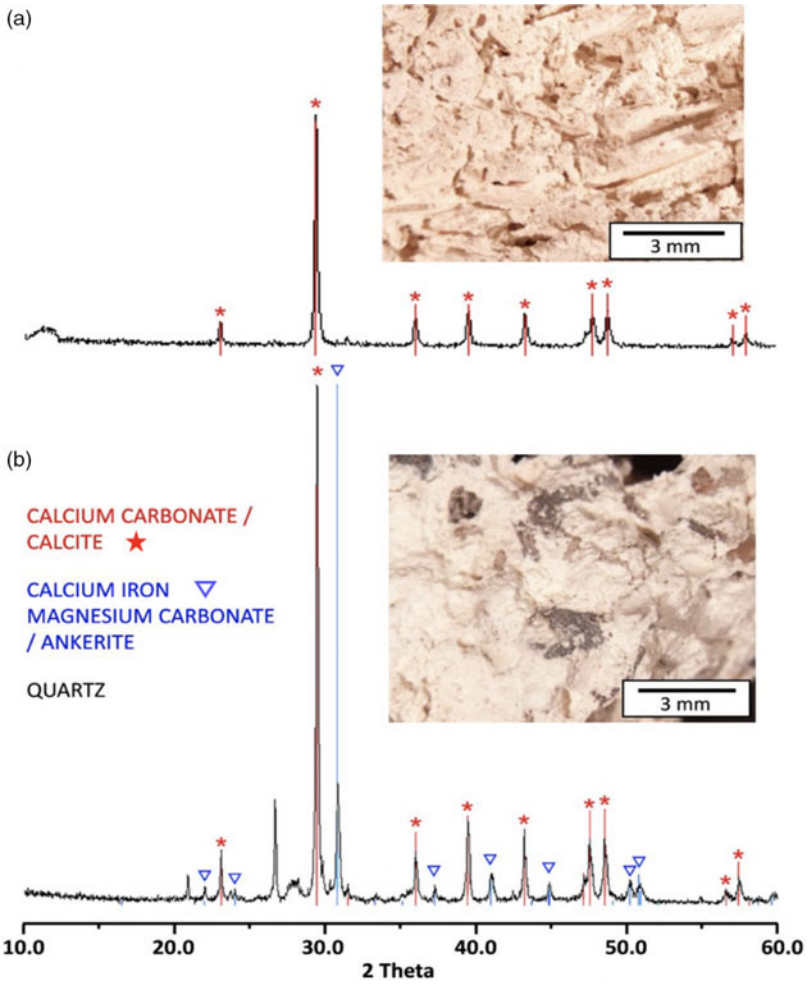

Figure 1 Macrophotographs of bulk samples, and XRD results of grain fraction 63–80 μm, of samples Hip10 (a) and Hip61 (b). Samples Hip8 and Hip10 had a similar composition and XRD pattern, independently from a chosen fraction.

(Figure 1a). The mortar Hip61 contained different kinds of aggregate, mainly carbonaceous and basaltic (Figure 1b). Petrography of the samples was previously described in (Michalska Nawrocka et al. 2007; Kabacińska et al. 2014b; Michalska and Pawlyta 2019). The raw material for their production was the rocks of the Hordos Formation, occurring in the vicinity of Hippos (Michalska and Pawlyta 2019). XRD results showed homogeneous structure of sample Hip10 and Hip8 (Figure 1a) and different sources of carbonates, namely $CaCO_3$ and $CaMgFeCO_3$, and additionally the presence of quartz in mortar Hip61 (Figure 1b).

Identification of Paramagnetic Centers

Full-range EPR spectra (650 mT magnetic field sweep) of investigated samples were previously shown and described in Kabacińska et al. (2014b). They are characterized by a presence of

https://doi.org/10.1017/RDC.2020.48 Published online by Cambridge University Press

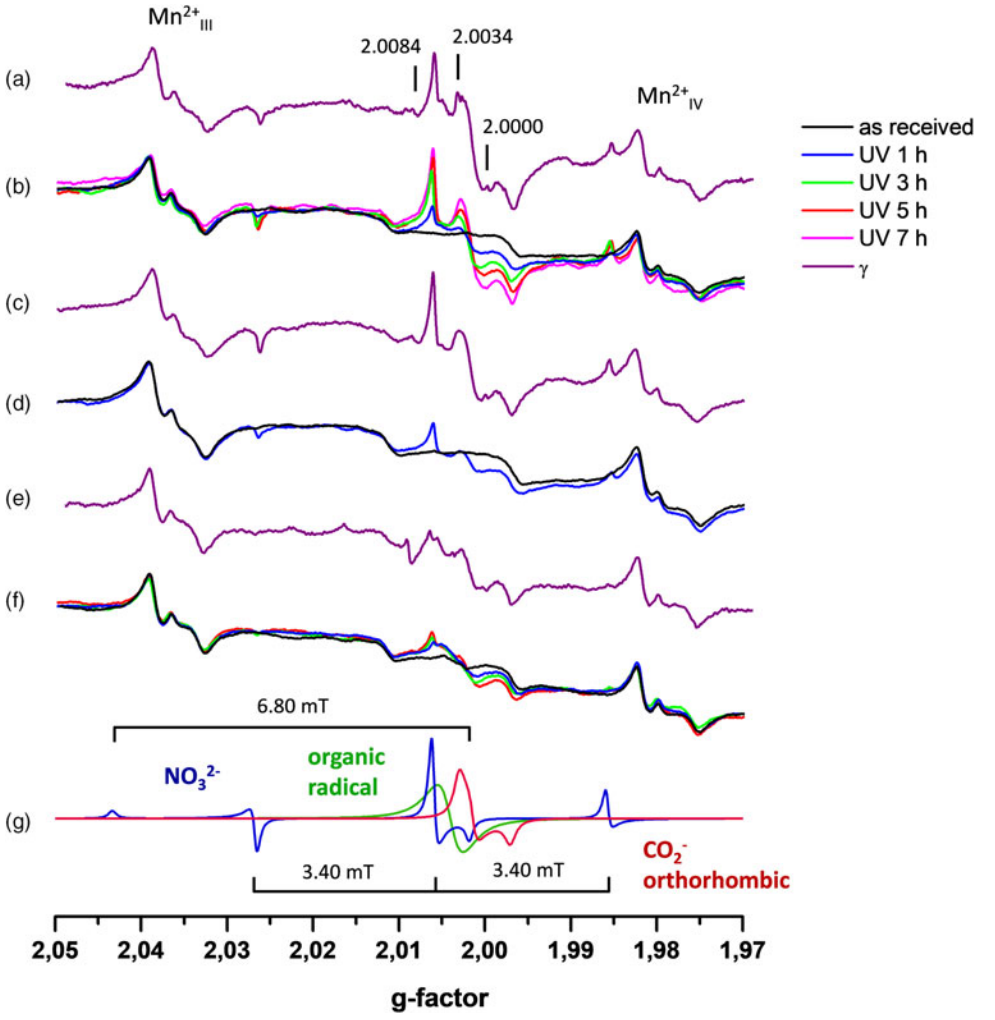

Figure 2 EPR spectra of UV- and γ-irradiated samples Hip10 (a, b), Hip8 (c, d) and 61H (e, f), and simulated signals present in those spectra (g). γ dose for samples Hip10 and Hip8 was 1 kGy, and 2.21 kGy for sample 61H. Spectra were normalized using Mn^{2+} signal as a reference.

common impurities—iron (*g*-factor values $g_a = 4.240$ and $g_b = 2.032$) (Ikeya 1993; Polikreti et al. 2004) and manganese ions (Ikeya 1993; Baïetto et al. 1999; Polikreti et al. 2004).

Figure 2 and Figure S1 present the EPR spectra (15 mT range) of as-received and γ- and UV-irradiated samples Hip8, Hip10 and 61H. Both γ- and UV-irradiation induced two main overlapping signals in Hippos samples, shown as simulated lines in Figure 2g—a triplet resulting from hyperfine structure ($I = 1$), with parameters $g_x = g_y = 2.0060$, $g_z = 2.0019$, $A_x = A_y = 3.40$ mT, $A_z = 6.80$ mT, and an orthorhombic signal with $g_x = 2.0029$, $g_y = 2.0014$, $g_z = 1.9971$. While the latter is a well-known signal connected with CO_2^- paramagnetic center (Ikeya 1993, 2004; Callens et al. 1998; Bartoll et al. 2000), the triplet is assigned by several authors to NO_3^{2-} ion (Eachus and Symons 1968; De Cannière et al. 1988; Sato et al. 2004; Kundu et al. 2005; Sadło et al. 2015). Additionally, a wide, isotropic,

https://doi.org/10.1017/RDC.2020.48 Published online by Cambridge University Press

radiation-sensitive signal at $g = 2.0040$ was revealed with an aid of simulations, resembling the signal often referred to as an "organic radical" in carbonates (Grün and De Cannière 1984; Ikeya 1993, 2004; Callens et al. 1998; Kundu et al. 2005). As discussed by Callens et al. (1998), CO^{-} species can at least partially contribute to this signal. An isotropic signal at $g \approx 2.0084$, clearly visible in the spectra of γ-irradiated samples, became noticeable in the case of UV-exposed samples at higher UV doses. In tooth enamel a similar signal has been identified as organic carbon (Oduwole and Sales 1994) and in burned bones as the carbon radical (Wencka et al. 2005).

The presence of nitrates has been detected in some historical mortars and their possible sources were attributed to biological decomposition of wooden elements, the use of nitrate-containing additives in the production process to optimize the properties of the material, nitrate-producing bacteria due to e.g. contamination with bird droppings (Middendorf and Knöfel 2015), agricultural waste (Oguz et al. 2014), and acid waters (Thomson et al. 2004). The existence of nitrate deposits has been reported in some caves and deserts in hot and dry regions (De Cannière et al. 1988; Ikeya 1993; Kundu et al. 2005). In the case of mortars and plasters from Hippos the most likely explanation for the presence of nitrates is the decomposition of organic matter, such as straw added during the manufacturing process and the occurrence of nitrites in the desert evaporates. It is worth pointing out that nitrate impurities are not uncommon even in high-purity $CaCO_3$ samples (Kabacińska et al. 2019).

At least two more signals are present in the spectra of γ-irradiated samples (Figure 2 b, d, f): a narrow line at $g = 2.0034$ strongly overlapped by the orthorhombic CO_2^{-} signal, and a weak line at $g = 2.0000$. The first one is presumably connected with one of the carbonate species, such as axial CO_3^{3-} with $g = 2.0033$, $g = 2.0013$ (Eachus and Symons 1968; Callens 1997; Baïetto et al. 1999; Sato and Ikeya 2005; Sadło et al. 2015; Kabacińska et al. 2019), or alternatively with a SO_3– center with an axial ($g = 2.0034$, $g = 2.0019$) or isotropic ($g = 2.0031$) symmetry (Kai and Miki 1992; Ikeya 1993, 2004; Miki et al. 1993; Baïetto et al. 1999; Bartoll et al. 2000; Kabacińska et al. 2019). The signal at $g = 2.0000$, is described in the literature as a surface defect—electrons trapped at an CO_3^{2-} vacancy created by grinding (Grün 1991; Bahain et al. 1994; Bartoll et al. 2000; Kabacińska et al. 2017, 2019). However, as shown in Kabacińska et al. (2017, 2019), two kinds of this signal can be observed in calcite samples—with isotropic and orthorhombic/axial symmetry, and while the former is observed only in γ-irradiated materials, the latter is clearly visible, and relatively strong both after γ- and UV-irradiation, which points towards their different origin.

Radiation Response Curves

We investigated the effect of extending the UV-exposure on the samples, starting from 30 min, at which time the induced signals are already visible, and up to 7.5 hr of irradiation. The intensities of the three main signals: orthorhombic CO_2^{-}, NO_3^{2-} and organic radical were calculated by double integration of their simulated signals, and later plotted versus the time of UV-irradiation (Figure 3). Figure S2 shows an example of simulated spectrum and the individual signals. To obtain radiation response curves (also known as the growth curves) data were fitted with an exponential function following the equation: $N = N_s(1 - e^{-at})$, where: N – concentration of defects, N_s – saturation concentration, t – time of UV exposure, and a – the sensitivity coefficient, also understood as the probability of defect generation (fraction of unfilled traps that capture electrons per dose/time unit) (Grün 1991; Ikeya 1993, 2004). Since the irradiation was not continuous, but divided into 4 series, separated by a 1–10-week gap, measurement data from each session were fitted individually. After each gap,

https://doi.org/10.1017/RDC.2020.48 Published online by Cambridge University Press

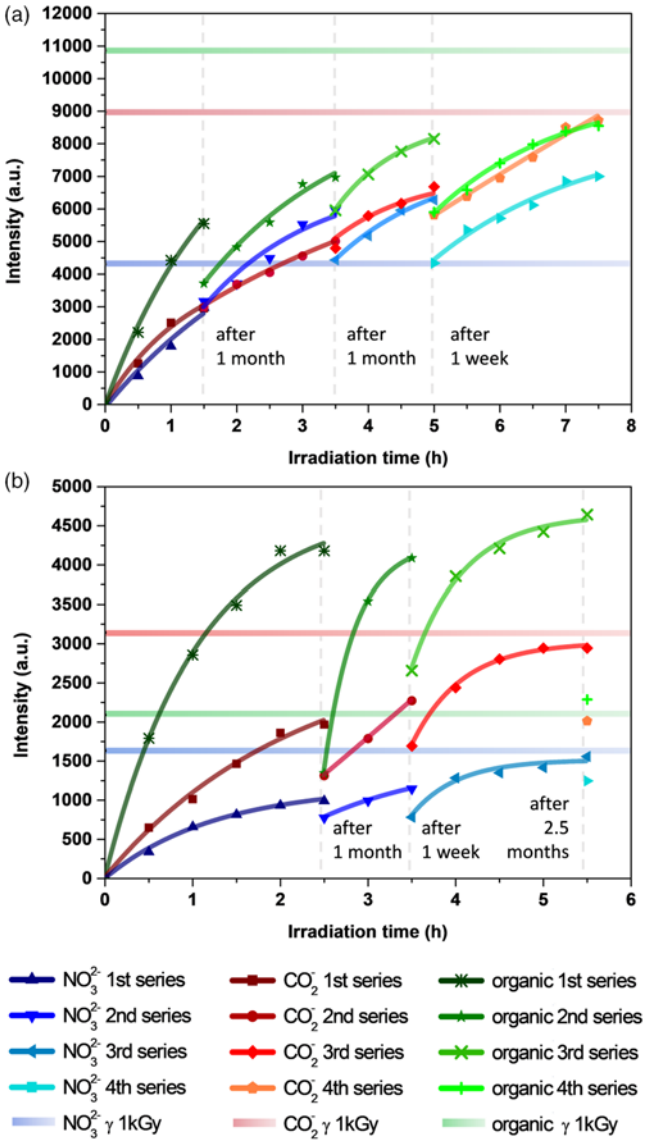

Figure 3 Radiation response curves for the signals observed in UV-irradiated samples Hip10 (a) and 61H (b). Horizontal lines correspond to intensities of γ-induced signals (1 kGy).

a significant decrease in the intensities was observed in most cases, due to partial recombination of generated paramagnetic species. However, the loss of intensity was quickly recovered in each session, and from the extrapolation of the curves we can determine that saturation of the signals would be reached generally after 5–6 hr of continuous irradiation.

Intensities of the signals induced by 1 kGy of γ radiation were presented in Figure 3 as horizontal lines. The radiation response curve for the orthorhombic CO_2^- species in γ-irradiated sample 61H was presented in Kabacińska et al. (2014b). It was shown therein

https://doi.org/10.1017/RDC.2020.48 Published online by Cambridge University Press

that saturation was reached around 20 kGy and for low doses (up to around 3 kGy) a linear function could describe the intensity growth. Comparing the intensities of γ- and UV-induced signals allows for estimation of an UV equivalent dose, understood as a dose reported in Gy (1 Gy = 1 J/kg) numerically equal to the absorbed dose of radiation from ^{60}Co source needed to generate the same signal intensity as observed after UV irradiation (Sholom et al. 2010). For the NO_3^{2-} species UV equivalent dose of 1 kGy would therefore correspond to ~2 hr and ~5 hr of continuous UV exposure for samples Hip10 and 61H respectively. The intensity of orthorhombic CO_2^- centers generated by 1 kGy of γ radiation is close to the saturation level of UV-induced signals, which can be observed after around 5 hr in both samples. For organic radical (or CO^- center) in sample 61H the same equivalent dose is reached after only 30 min of UV-irradiation, while for Hip10 would be reached after 6–7 hr of continuous irradiation, resulting in saturation of the signal.

It has to be borne in mind that due to a much smaller penetration depth of UV light compared to γ radiation (discussed in Kabacińska et al. 2019), resulting in slightly inhomogeneous irradiation of UV-exposed samples, the intensities observed in their cases can be underestimated. Additional considerations, such as using a very thin layer of powder and mixing it between irradiation sessions were included in order to minimize this effect, but one can assume that in an ideal scenario of a homogeneous irradiation the effect of UV light would be even more pronounced.

Stability of UV-Induced Centers

By analyzing the decrease in intensity of the signals between the irradiation sessions a few observations regarding the decay of the paramagnetic centers can be made. Radiation defects in sample Hip10 are characterized by higher stability, showing only up to 30% decrease, and in some cases (mainly orthorhombic CO_2^-) no changes in intensity between measurement sessions. Paramagnetic species in sample 61H display generally a 20–35% decrease, but for the organic radical a 50% and 70% drop was recorded for longer gaps. Stability of UV-induced signals in natural and synthetic high-purity calcite over an extended period of time after UV exposure was investigated in Kabacińska et al. 2019. While nitride defects described therein displayed similar stability (~20% decrease in 3 months), orthorhombic CO_2^- defects decayed faster, reaching half of their initial concentration after about a month from γ-irradiation, and about 3 months from UV-exposure. Several authors (Eachus and Symons 1968; De Cannière et al. 1988; Sato et al. 2004) determined the thermal stability of the NO_3^{2-} center to be significantly higher than for carbonate defects.

Mechanism

The presence of UV-induced signals in lime mortars confirms previous reports (Bartoll et al. 2000; Sato et al. 2004; Kundu et al. 2005; Kabacińska et al. 2014a, 2017, 2019), showing that radiation defects in carbonates can also be generated, instead of bleached by UV radiation. From the physical point of view, the most intriguing aspect of this phenomenon is the mechanism of their generation by UV light. It has to be borne in mind that in order to create a paramagnetic center the radiation incident on a crystal must have sufficient energy, which in case of calcite means higher than ~6 eV (band gap of calcite; Baer and Blanchard 1993). Since the UV radiation used in this study had lower energy, it could not directly excite electrons of carbonate groups to create carbonate defects. In Kabacińska et al. (2017, 2019) a mechanism of UV-induced generation of carbonate paramagnetic species in calcite

https://doi.org/10.1017/RDC.2020.48 Published online by Cambridge University Press

based on re-trapping the so-called "secondary electrons" from non-carbonate traps was proposed. We use the term "secondary electrons" (with quotation marks), first used in this context by Baran et al. (2011), to describe the electrons released by UV light, therefore they should not be understood as electrons generated by ionization, which is the normal definition of secondary electrons. Some of the non-carbonate electron traps can be formed in the crystal prior to UV exposure, and others directly by UV irradiation, provided the energy required for excitation is lower than calcite band gap. Moreover, specific impurities, such as Mn, Zn, and Mg can enhance the trapping process, acting as activators and sensitizers. This mechanism explains the saturation of UV-induced radiation defects at a relatively low level (compared to γ) by exhausting the supply of "secondary electrons".

The efficiency of the generation process was shown to be strongly connected with the size and morphology of calcite grains. Lime mortars, characterized by relatively big grains (sample 61H is a sieved fraction 63–80 μm, Hip8 and Hip10 were not sieved) with considerable amount of impurities, resemble some of the samples described in Kabacińska et al. (2019) (classified therein as "Group II" samples) and a powdered natural single crystal of calcite investigated in Kabacińska et al. 2017. Their common feature is a relatively high sensitivity to UV radiation (1 hr of UV exposure is equivalent to few hundreds Gy of γ dose) and presence of the same signals after UV- as after γ-irradiation. It was postulated that a big grain size, resulting in smaller specific surface area and therefore limiting the recombination of excited electrons, facilitates diffusion of excited charges in the material, while the impurities provide the "secondary electrons" and enhance the trapping process, leading to efficient creation of carbonate paramagnetic centers. At the same time, the presence of NO_3^- ions in mortars from Hippos is also the distinctive characteristic of three of the samples from Kabacińska et al. 2019, classified as "Group III". Several authors, reported on NO_3^- ions acting as very efficient electron traps in irradiated calcite (Eachus and Symons 1968; De Cannière et al. 1988; Sato et al. 2004; Kundu et al. 2005) and hydroxyapatite (Baran et al. 2011), nitrate species can therefore be a good source of "secondary electrons" for carbonate centers.

Implication for Mortar Dating

Our results confirm that in lime mortars, like in other carbonate materials, various radiation defects are generated when the material is subjected to irradiation. The fact that calcium carbonate crystalizes during the hardening of a binder, at which point all the electron traps are empty, means that, in theory, a well-chosen sample could give the age of a mortar through EPR dating. However, too-young materials will not give a measurable EPR signal, which has to be taken into account when selecting the samples. A detailed and systematic investigation of the structure and dynamics of the paramagnetic centers in the binder and the aggregate (in which the traps were not emptied during the manufacturing process) is necessary for finding the radiation defects that best reflect the age of the mortar, without the need of mechanically removing the aggregate. Despite the very preliminary status of EPR application in mortar dating, we believe that its potential as another source of valuable information is certainly worth further studies.

While the effects of sunlight and other weathering conditions on lime mortars and plasters are the subject of thorough investigation, their influence has never been considered in terms of generation of radiation defects in calcium carbonate. Our observations open a new possibility of employing a well-established "clock" based on trapped-charges to determine the period of exposure of the material to sunlight instead of ionizing radiation. The fact that UV light constitutes only a small portion of sunlight spectrum reaching the Earth's

https://doi.org/10.1017/RDC.2020.48 Published online by Cambridge University Press

surface would make the efficiency of defect generation much smaller, extending the time before reaching saturation, hopefully to a period relevant for age determination. Naturally, partial bleaching of newly created paramagnetic centers, and a number of other factors have to be also considered before estimating the applicability of this approach. Studies of sunlight's effect on calcium carbonate, aided by the tremendous potential of EPR spectroscopy, are vital to fully understand the physical mechanism of those processes, and consequently to utilize the radiation defect-generating properties of UV light in mortar analysis.

SUMMARY

Using EPR spectroscopy we examined the effect of γ and UV irradiation on lime mortars and plasters from the ancient settlement Hippos in Israel. Using an artificial UV source we generated relatively strong signals of paramagnetic centers, analogous to those created by γ irradiation, reaching their maximum intensity after 5–6 hr of UV exposure. Both types of radiation induced the centers identified as CO_2^-, NO_3^{2-} and organic radical. Our observations of UV-induced generation of carbonate paramagnetic species in lime mortars can be explained using a mechanism based on re-trapping the "secondary electrons", i.e. the electrons released from non-carbonate traps by UV light. Big grain size and the high amount of impurities in the material facilitate this process. Exhausting the supply of "secondary electrons" explain the saturation of UV-induced signals at a relatively low level compared to γ-irradiation. Our results confirm that radiation defects can also be generated, instead of bleached, in calcite by UV radiation, presenting new aspects of mortar research.

ACKNOWLEDGMENTS

The authors would like to gratefully thank Prof. J. Młynarczyk (Institute of Archaeology, University of Warsaw), Dr. M. Burdajewicz (National Museum in Warsaw), and Prof. A. Segal (Zinman Institute of Archaeology, University of Haifa), for invitation to participate in excavation and the possibility to collect the mortar and plaster samples for further analyses and dating. Samples were γ-irradiated at the Institute of Applied Radiation Chemistry, Technical University of Łódź and the Institute of Molecular Physics, Polish Academy of Sciences in Poznań, with kind help of Dr. M. Wencka. This work has been partially supported by the funds of the Ministry of Science and Higher Education by grants No. IP2010027870 and No. N N307 059437, and Human Capital Operational Programme of the Polish National Centre for Research and Development (NCBR) - PO KL 4.1.1 "Proinnowacyjne kształcenie, kompetentna kadra, absolwenci przyszłości" ("Pro-innovation training, competent staff, graduates of the future").

SUPPLEMENTARY MATERIAL

To view supplementary material for this article, please visit https://doi.org/10.1017/RDC.2020.48

REFERENCES

Baer DR, Blanchard DL. 1993. Studies of the calcite cleavage surface for comparison with calculation. Applied Surface Science 72(4):295–300. doi: 10.1016/0169-4332(93)90365-I.

Bahain J-J, Yokoyama Y, Masaoudi H, Falguéres C, Laurent M. 1994. Thermal behaviour of ESR signals observed in various natural carbonates. Quaternary Science Reviews 13(5–7):671–674. doi: 10.1016/0277-3791(94)90096-5.

Baïetto V, Villeneuve G, Schvoerer M, Bechtel F, Herz N, Baietto V, Villeneuve G, Schvoerer M, Bechtel F, Herz N. 1999. Investigation of

electron paramagnetic resonance peaks in some powdered Greek white marbles. Archaeometry 412(2):253–265.

Baran NP, Vorona IP, Ishchenko SS, Nosenko VV, Zatovskii IV, Gorodilova NA, Povarchuk VY. 2011. NO_3^{2-} and CO_2^{-} centers in synthetic hydroxyapatite: Features of the formation under γ- and UV-irradiations. Physics of the Solid State 53(9):1891–1894. doi: 10.1134/S106378341109006X.

Bartoll J, Stößer R, Nofz M. 2000. Generation and conversion of electronic defects in calcium carbonates by UV/Vis light. Applied Radiation and Isotopes 52(5):1099–1105. doi: 10.1016/S0969-8043(00)00044-0.

Callens F, Vanhaelewyn G, Matthys P, Boesman E. 1998. EPR of carbonate derived radicals: Applications in dosimetry, dating and detection of irradiated food. Applied Magnetic Resonance 14(2–3):235–254. doi: 10.1007/BF03161892.

Callens FJ. 1997. Comparative EPR and endor results on carbonate derived radicals in different host materials. Nukleonika 42(2):565–578.

De Cannière P, Debuyst R, Dejehet F, Apers D. 1988. ESR study of internally α-irradiated (^{210}Po nitrate doped) calcite single crystal. International Journal of Radiation Applications and Instrumentation. Part D. Nuclear Tracks and Radiation Measurements 14(1–2):267–273. doi: 10.1016/1359-0189(88)90075-1.

Eachus RS, Symons MCR. 1968. Unstable intermediates. Part L. The NO32- impurity centre in irradiated calcium carbonate. Journal of the Chemical Society A: Inorganic, Physical, Theoretical 437(124):790. doi: 10.1039/j19680000790.

Grün R. 1991. Potential and problems of ESR dating. International Journal of Radiation Applications and Instrumentation. Part D. Nuclear Tracks and Radiation Measurements 18(1–2):143–153. doi: 10.1016/1359-0189(91)90106-R.

Grün R, De Cannière P. 1984. ESR-dating: Problems encountered in the evaluation of the naturally accumulated dose /AD/ of secondary carbonates. Journal of Radioanalytical and Nuclear Chemistry 85(4):213–226. doi: 10.1007/BF02164225.

Hajdas I, Lindroos A, Heinemeier J, Ringbom Å, Marzaioli F, Terrasi F, Passariello I, Capano M, Artioli G, Addis A, et al. 2017. Preparation and Dating of Mortar Samples-Mortar Dating Inter-Comparison Study (MODIS). Radiocarbon 59(6):1845–1858. doi: 10.1017/RDC.2017.112.

Ikeya M. 1993. New applications of electron spin resonance: Dating, dosimetry and microscopy. Singapore, New Jersey, London, Hong Kong: World Scientific.

Ikeya M. 2004. ESR dating, dosimetry and microscopy for terrestrial and planetary materials. Electron Paramagnetic Resonance 19:1–32. doi: 10.1002/chin.200519298.

Kabacińska Z, Krzyminiewski R, Dobosz B. 2014a. EPR investigation of UV light effect on calcium carbonate powders with different grain sizes. Radiation Protection Dosimetry 159(1–4):149–154. doi: 10.1093/rpd/ncu177.

Kabacińska Z, Krzyminiewski R, Dobosz B, Nawrocka D. 2012. ESR investigation of structure and dynamics of paramagnetic centres in lime mortars from Budinjak, Croatia. Radiation Measurements 47(9):825–829. doi: 10.1016/j.radmeas.2012.03.017.

Kabacińska Z, Krzyminiewski R, Michalska D, Dobosz B. 2014b. Investigation of lime mortars and plasters from archaeological excavations in Hippos (Israel) using electron paramagnetic resonance. Geochronometria 41(2):112–120. doi: 10.2478/s13386-013-0151-4.

Kabacińska Z, Krzyminiewski R, Tadyszak K, Coy E. 2019. Generation of UV-induced radiation defects in calcite. Quaternary Geochronology 51(August 2018):24–42. doi: 10.1016/j.quageo.2019.01.002.

Kabacińska Z, Yate L, Wencka M, Krzyminiewski R, Tadyszak K, Coy E. 2017. Nanoscale effects of radiation (UV, X-ray, and γ) on calcite surfaces: Implications for its mechanical and physico-chemical properties. The Journal of Physical Chemistry C 121(24):13357–13369. doi: 10.1021/acs.jpcc.7b03581.

Kai A, Miki T. 1992. Electron spin resonance of sulfite radicals in irradiated calcite and aragonite. International Journal of Radiation Applications and Instrumentation. Part C. Radiation Physics and Chemistry 40(6):469–476. doi: 10.1016/1359-0197(92)90211-W.

Kundu HK, Sato H, Ganas A, Ikeya M. 2005. ESR studies on calcite encrustation on Fili Neotectonic Fault, Greece. Applied Magnetic Resonance 29:185–194.

Michalska D. 2019. Influence of different pretreatments on mortar dating results. Nuclear Instruments and Methods in Physics Research B 456:236–246. doi: 10.1016/j.nimb.2019.03.038.

Michalska D, Czernik J, Goslar T. 2017. Methodological aspect of mortars dating (Poznań, Poland, MODIS). Radiocarbon 59(6):1891–1906. doi: 10.1017/RDC.2017.128.

Michalska D, Pawlyta J. 2019. Modeled and measured carbon isotopic composition and petrographically estimated binder-aggregate ratio—recipe for binding material dating? Radiocarbon 61(3):799–815. doi: 10.1017/RDC.2019.29.

Michalska Nawrocka D, Michczyńska DJ, Pazdur A, Czernik J. 2007. Radiocarbon chronology of the ancient settlement in the Golan Heights Area, Israel. Radiocarbon 49(2):625–637. doi: 10.1017/S0033822200042521.

Middendorf B, Knöfel D. 2015. Characterization of historic mortars from building in Germany and the Netherlands. In: Baer N, Fitz S, Livingstone RA, editors. Conservation of historic brick structures. Routledge.

https://doi.org/10.1017/RDC.2020.48 Published online by Cambridge University Press

Miki T, Kai A, Murata T. 1993. Radiation-induced radicals in sulfite-doped $CaCO_3$. Applied Radiation and Isotopes 44(1–2):315–319. doi: 10.1016/0969-8043(93)90238-6.

Nawrocka D, Czernik J, Goslar T. 2009. ^{14}C dating of carbonate mortars from Polish and Israeli sites. Radiocarbon 51(02):857–866. doi: 10.1017/S0033822200056162.

Nawrocka D, Michniewicz J, Pawlyta J. 2005. Application of radiocarbon method for dating of lime mortars. Geochronometria 24:109–115.

Oduwole AD, Sales KD. 1994. Transient ESR signals induced by γ-irradiation in tooth enamel and in bone. Quaternary Science Reviews 13(5–7): 647–650. doi: 10.1016/0277-3791(94)90093-0.

Oguz C, Turker F, Kockal NU. 2014. Construction materials used in the historical Roman Era bath in Myra. The Scientific World Journal 2014:1–9. doi: 10.1155/2014/536105.

Panzeri L. 2013. Mortar and surface dating with optically stimulated luminescence (OSL): Innovative techniques for the age determination of buildings. Nuovo Cim della Soc Ital di Fis C. 36(April):205–216. doi: 10.1393/ncc/i2013-11555-9.

Polikreti K, Maniatis Y, Bassiakos Y, Kourou N, Karageorghis V. 2004. Provenance of archaeological limestone with EPR spectroscopy: The case of the Cypriote-type statuettes. Journal of Archaeological Science 31:1015–1028. doi: 10.1016/j.jas.2003.12.013.

Ringbom Å, Lindroos A, Heinemeier J, Sonck-Koota P. 2014. 19 Years of mortar dating: learning from experience. Radiocarbon 56(2):619–635. doi: 10.2458/56.17469.

Sadło J, Bugaj A, Strzelczak G, Sterniczuk M, Jaegermann Z. 2015. Multifrequency EPR study on radiation induced centers in calcium carbonates labeled with ^{13}C. Nukleonika 60(3):429–434. doi: 10.1515/nuka-2015-0076.

Sato H, Ikeya M. 2005. Possibility of precipitated CaCO 3 with vitamin C as a new dosimetric material. Applied Radiation and Isotopes 62:337–341. doi: 10.1016/j.apradiso.2004.08.025.

Sato H, Tani A, Fielding AJ, Eaton SS, Eaton GR, Whitehead NE, Ikeya M. 2004. Spatial distribution and formation of nitrate radical NO32− in Antarctic calcitic evaporates. Applied Magnetic Resonance 26(4):601–616. doi: 10.1007/BF03166586.

Sholom S, Desrosiers M, Chumak V, Luckyanov N, Simon SL, Bouville A. 2010. UV Effects in tooth enamel and their possible application in EPR dosimetry with front teeth. Health Physics 98(2): 360–368. doi: 10.1097/01.HP.0000348002.69740.bd.

Thomson ML, Lindqvist J-E, Elsen J, Groot CJWP. 2004. Origin of porosity in mortars. In: Martens D, Vermeltfoort A, editors. 13th International Brick and Block Masonry Conference. Technische Universiteit Eindhoven. p. 1–10.

Urbanová P, Guibert P. 2017. Methodological study on single grain OSL dating of mortars: comparison of five reference archaeological sites. Geochronometria 44:77–97. doi: 10.1515/geochr-2015-0050.

Wencka M, Hoffmann SK, Hercman H. 2005. EPR dating of hydroxyapatite from fossil bones. Transient effects after γ and UV irradiation. Acta Physica Polonica A 108(2):331–337.

https://doi.org/10.1017/RDC.2020.48 Published online by Cambridge University Press